J|A|C|S
ARTICLES

Published on Web 06/21/2008

Femtosecond Fluorescence and Intersystem Crossing in Rhenium(I) Carbonyl−Bipyridine Complexes

Andrea Cannizzo,[†] Ana Maria Blanco-Rodríguez,[‡] Amal El Nahhas,[†] Jakub Šebera,[§] Stanislav Záliš,[*,§] Antonín Vlček, Jr.,[*,‡,§] and Majed Chergui[*,†]

Laboratoire de Spectroscopie Ultrarapide, ISIC, FSB-BSP, Ecole Polytechnique Fédérale de Lausanne, CH-1015 Lausanne-Dorigny, Switzerland, School of Biological and Chemical Sciences, Queen Mary, University of London, Mile End Road, London E1 4NS, United Kingdom, and J. Heyrovský Institute of Physical Chemistry, Academy of Sciences of the Czech Republic, Dolejškova 3, CZ-182 23 Prague, Czech Republic

Received December 12, 2007; E-mail: Majed.Chergui@epfl.ch; a.vlcek@qmul.ac.uk; zalis@jh-inst.cas.cz

Abstract: Ultrafast electronic-vibrational relaxation upon excitation of the singlet charge-transfer b^1A' state of $[Re(L)(CO)_3(bpy)]^n$ (L = Cl, Br, I, $n = 0$; L = 4-Et-pyridine, $n = 1+$) in acetonitrile was investigated using the femtosecond fluorescence up-conversion technique with polychromatic detection. In addition, energies, characters, and molecular structures of the emitting states were calculated by TD-DFT. The luminescence is characterized by a broad fluorescence band at very short times, and evolves to the steady-state phosphorescence spectrum from the a^3A'' state at longer times. The analysis of the data allows us to identify three spectral components. The first two are characterized by decay times $\tau_1 = 85-150$ fs and $\tau_2 = 340-1200$ fs, depending on L, and are identified as fluorescence from the initially excited singlet state and phosphorescence from a higher triplet state (b^3A''), respectively. The third component corresponds to the long-lived phosphorescence from the lowest a^3A'' state. In addition, it is found that the fluorescence decay time (τ_1) corresponds to the intersystem crossing (ISC) time to the two emissive triplet states. τ_2 corresponds to internal conversion among triplet states. DFT results show that ISC involves electron exchange in orthogonal, largely Re-localized, molecular orbitals, whereby the total electron momentum is conserved. Surprisingly, the measured ISC rates scale inversely with the spin−orbit coupling constant of the ligand L, but we find a clear correlation between the ISC times and the vibrational periods of the Re−L mode, suggesting that the latter may mediate the ISC in a strongly nonadiabatic regime.

I. Introduction

Controlling the behavior of singlet and triplet metal-to-ligand charge transfer (^{1}MLCT and ^{3}MLCT, respectively) excited states of transition metal complexes is key to their efficient use in photonic applications. For example, operation of Ir^{III} luminophores in organic light-emitting diodes (OLED),[1,2] Ru^{II}-based sensitizers of solar cells,[3,4] Re^{I} probes of protein relaxation dynamics,[5] or various luminescence sensors are all based on the presence of ^{3}MLCT states. Optical excitation of metal-containing chromophores prepares ^{1}MLCT states, from which the strongly phosphorescent triplet states are populated by intersystem crossing (ISC). Apart from this role as an optical gateway, ^{1}MLCT states can be exploited in ultrafast chemical processes such as electron injection, energy transfer, or metal−ligand bond dissociation, which can compete with ISC.

Understanding the character and dynamics of optically excited ^{1}MLCT states presents a considerable challenge to contemporary photophysical research, as they are often very short-lived. Singlet−triplet (and also doublet-quartet) ISC rates were determined only in few cases and found to range from tens of femtoseconds to a few picoseconds.[6−14] ^{1}MLCT fluorescence lifetimes of the generic photosensitizers $[Ru^{II}(bpy)_3]^{2+}$ and $[Ru(4,4'\text{-}(COOH)_2\text{-}bpy)_2(NCS)_2]$ (N3) were recently measured

[*] To whom correspondence should be addressed.
[†] Laboratoire de Spectroscopie Ultrarapide, ISIC, FSB-BSP, Ecole Polytechnique Fédérale de Lausanne, CH-1015 Lausanne-Dorigny, Switzerland.
[‡] School of Biological and Chemical Sciences, Queen Mary, University of London, Mile End Road, London E1 4NS, United Kingdom.
[§] J. Heyrovský Institute of Physical Chemistry, Academy of Sciences of the Czech Republic, Dolejškova 3, CZ-182 23 Prague, Czech Republic.

(1) Evans, R. C.; Douglas, P.; Winscom, C. J. *Coord. Chem. Rev.* **2006**, *250*, 2093.
(2) Yersin, H. Triplet Emitters for OLED Applications. Mechanisms of Exciton Trapping and Control of Emission Properties In Topics in Current Chemistry. *Transition Metal and Rare Earth Compounds*; Springer: New York, 2004; Vol. 241; pp 1.
(3) Hagfeldt, A.; Grätzel, M. *Acc. Chem. Res.* **2000**, *33*, 269.
(4) Grätzel, M. *Nature* **2001**, *414*, 338.
(5) Blanco-Rodríguez, A. M.; Busby, M.; Grădinaru, C.; Crane, B. R.; Di Bilio, A. J.; Matousek, P.; Towrie, M.; Leigh, B. S.; Richards, J. H.; Vlček, A., Jr.; Gray, H. B. *J. Am. Chem. Soc.* **2006**, *128*, 4365.
(6) Cannizzo, A.; van Mourik, F.; Gawelda, W.; Zgrablic, G.; Bressler, C.; Chergui, M. *Angew. Chem., Int. Ed.* **2006**, *45*, 3174.
(7) Gawelda, W.; Cannizzo, A.; Pham, V.-T.; van Mourik, F.; Bressler, C.; Chergui, M. *J. Am. Chem. Soc.* **2007**, *129*, 8199.
(8) McFarland, S. A.; Lee, F. S.; Cheng, K. A. W. Y.; Cozens, F. L.; Schepp, N. P. *J. Am. Chem. Soc.* **2005**, *127*, 7065.
(9) Bhasikuttan, A. C.; Okada, T. *J. Phys. Chem. B* **2004**, *108*, 12629.
(10) Siddique, Z. A.; Ohno, T.; Nozaki, K. *Inorg. Chem.* **2004**, *43*, 663.
(11) Siddique, Z. A.; Yamamoto, Y.; Ohno, T.; Nozaki, K. *Inorg. Chem.* **2003**, *42*, 6366.
(12) Burdzinski, G. T.; Ramnauth, R.; Chisholm, M. H.; Gustafson, T. L. *J. Am. Chem. Soc.* **2006**, *128*, 6776.
(13) Monat, J. E.; McCusker, J. K. *J. Am. Chem. Soc.* **2000**, *122*, 4092.
(14) Juban, E. A.; McCusker, J. K. *J. Am. Chem. Soc.* **2005**, *127*, 6857.

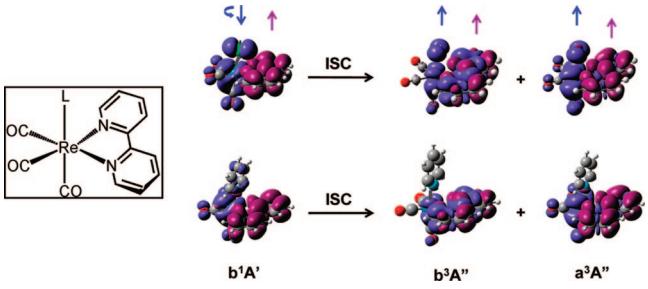

Figure 1. Visualization of the singlet and triplet excited states and intersystem crossing in $[Re(Cl)(CO)_3(bpy)]$ (top) and $[Re(py)(CO)_3(bpy)]^+$ (bottom) using difference electron density maps calculated by TD-DFT (B3LYP, singlets in CH_3CN/CPCM, triplets for L = Cl in CH_3CN (CPCM), L = py in vacuum). Cl or py ligands point up. The plots show the electron density in the given excited-state minus electron density in the ground state, at the optimized ground-state geometry. Blue, violet: regions where electron density decreases and increases upon excitation, respectively. These regions approximately correspond to those occupied by the two unpaired electrons in the excited states, shown by the arrows at the top. Orbital rotation accompanying the spin change is clearly seen. Inset: schematic molecular structure of the investigated complexes.

to be 20 fs and 43 ± 10 fs, respectively.[6,9] For $[Ru^{II}(bpy)_3]^{2+}$ and $[Fe^{II}(bpy)_3]^{2+}$, the ^{3}MLCT phosphorescence intensity rises with the same (≤20 fs) kinetics, indicating an unusually ultrafast ^{1}MLCT → ^{3}MLCT ISC.[6,7] The observation that the ^{1}MLCT lifetime in Fe and Ru tris-bipyridine[6,7] complexes is comparable to the period of highest-frequency vibrations of the bpy ligand demonstrates the breakdown of the traditional "cascade" model of excited-state dynamics, whereby the electronic states decay through a sequence of steps (vibrational relaxation, internal conversion, ISC, etc.) that are well separated in time and energy. Instead, we are dealing with convoluted electronic relaxation, spin change, and vibrational energy redistribution on strongly coupled potential energy surfaces. The fact that the ISC rate does not decrease with the spin−orbit coupling (SO) constant of the metal in isostructural Fe and Ru tris-bipyridine complexes raised the question of the role of structural dynamics in nonadiabatic ISC.[7] Understanding the effects which control ISC and population of emissive triplet states in metal complexes clearly requires investigating the dependence of the ISC dynamics on the metal atom, as well as composition and symmetry of the coordination sphere.

Here, we report on the first observation of fluorescence from optically populated ^{1}CT (charge transfer) states of rhenium(I) complexes $[Re(L)(CO)_3(bpy)]^n$ (L = Cl, Br, I, n = 0; L = 4-Ethyl-pyridine (Etpy), n = 1+), which contain a single, well-localized electron-accepting bpy ligand (see inset of Figure 1). Furthermore, Re has a larger SO constant than Fe and Ru, and coordination with a halide ligand should further enhance the SO coupling, while this is not the case with L = Etpy. Using femtosecond broadband fluorescence up-conversion techniques,[6,15,16] we present evidence that intersystem crossing (ISC) populates simultaneously two phosphorescent ^{3}MLCT states on a time scale of ∼100 fs. Surprisingly, the ISC rates are found to be slower than in $[M^{II}(bpy)_3]^{2+}$ (M=Ru, Fe) complexes,[6,7] and they do not scale with the SO constant of the L ligand. A theoretical (TD-DFT) description of the low-lying singlet and triplet CT states is presented, which allows us to propose an explanation of the ISC occurrence and rates. The observations of the fluorescence and early phosphorescence in Re^I complexes and the proposed interpretation based on first-order spin−orbit coupling and promoting vibrations have implications for the photophysics and for photonic applications of transition metal complexes and organometallics.

II. Experimental Section

II.1. Materials. The complexes $[Re(X)(CO)_3(bpy)]$ (X = Cl, Br) and $[Re(Etpy)(CO)_3(bpy)]PF_6$ were synthesized and characterized by previously published procedures.[17,18] $[Re(I)(CO)_3(bpy)]$ was synthesized by reacting a photochemically prepared[19] mixture of $[Re(CO)_5I]$ and $[Re(CO)_4I]_2$ with bpy: $Re_2(CO)_{10}$ (0.74 g., 1.13 mmol) and iodine (0.44 g, 1.71 mmol) were added to degassed anhydrous hexane (60 mL). The solution was purged with CO for 10 min before being irradiated with a medium-pressure Hg lamp for 4 h. The solvent was removed under vacuum and the resulting solid was dissolved in ethanol (10 mL). A solution of $Na_2S_2O_3$ (0.3 g) in water (10 mL) was added to remove excess iodine. The resulting solid containing $[Re(CO)_5I]$ with a smaller amount of $[Re(CO)_4I]_2$ was filtered, washed with water, and dried. It was then reacted with excess 2,2′-bipyridine (∼5 molar equiv) in toluene (8 mL) at 80 °C for 3 h. Both $[Re(CO)_5I]$ and $[Re(CO)_4I]_2$ were almost quantitatively converted to $[Re(I)(CO)_3(bpy)]$, which was filtered, washed with petroleum ether and characterized[18] by IR, UV−vis, and phosphorescence spectra. A spectroscopic grade acetonitrile (CH_3CN) solvent was used as obtained from Aldrich.

II.2. Time-Resolved Luminescence Spectra. A broadband femtosecond fluorescence up-conversion setup, described previously,[15,16] was used to detect time-resolved luminescence spectra in the 440−680 nm range, with a resolution of ∼100 fs. The samples were excited with 80 fs, 400 nm pulses having an energy of 16 nJ/pulse, in a focal spot of 50 μm (fwhm), and at a repetition rate of 250 kHz. Under these conditions, no photodegradation of the samples was observed. The luminescence, collected in forward scattering geometry, is up-converted in a 250 μm thick β Barium Borate (BBO) crystal by mixing with an 800 nm gate pulse. The up-converted signal is spatially filtered and detected with a spectrograph and a liquid-N_2 cooled CCD camera in polychromatic mode. The collected luminescence signal was corrected for the Group Velocity Dispersion (GVD) over the entire detection range (the blue-most component is delayed by ∼400 fs with respect to the red-most component). The GVD was measured by recording a white light pulse signal generated in a neat water solution at the same experimental conditions. The reported luminescence spectra have not been corrected for the spectral response of the detection system. Color filters were used to attenuate the remaining 400 and 800 nm light. This greatly improves the signal-to-noise ratio but limits the detectable spectral range to the 440−680 nm region. Time zero was determined by detecting the up-converted Raman line of the solvent at 457 nm. The sample was flown in a 0.5-mm thick quartz flow cell at a speed of 1 m/s to avoid photodegradation. With the above experimental conditions, the 400 nm pulse hits the same spot ∼10 times. However, since the lifetime of the lowest excited state (triplet ^{3}MLCT state) is much less

(15) Zgrablić, G.; Voitchovsky, K.; Kindermann, M.; Haacke, S.; Chergui, M. *Biophys. J.* **2005**, *88*, 2779.
(16) Cannizzo, A.; Bräm, O.; Zgrablic, G.; Tortschanoff, A.; Ajdarzadeh Oskouei, A.; van Mourik, F.; Chergui, M. *Opt. Lett.* **2007**, *32*, 3555.
(17) Hino, J. K.; Della Ciana, L.; Dressick, W. J.; Sullivan, B. P. *Inorg. Chem.* **1992**, *31*, 1072.
(18) Rossenaar, B. D.; Stufkens, D. J.; Vlček, A., Jr. *Inorg. Chem.* **1996**, *35*, 2902.
(19) Schmidt, S. P.; Trogler, W. C.; Basolo, F. In *Inorganic Syntheses*; Angelici, R. J., Ed.;J. Wiley: New York, 1990; Vol. 28.

than 1 μs, all of the excited molecules relax to the ground-state between two successive excitation pulses.

II.3. Quantum Chemical Calculations. The electronic structures of $[Re(Cl)(CO)_3(bpy)]$, $[Re(I)(CO)_3(bpy)]$, and $[Re(py)(CO)_3(bpy)]^+$ (which represents $[Re(Etpy)(CO)_3(bpy)]^+$) were calculated by density functional theory (DFT) methods using the Gaussian 03[20] and Turbomole[21,22] program packages. DFT calculations employed hybrid functionals; either B3LYP[23] or Perdew, Burke, and Ernzerhof[24,25] (PBE0). The solvent was described by the polarizable conductor calculation model (CPCM)[26] (G03) or conductor-like screening model[27,28] (COSMO) (Turbomole). Low-lying singlet and triplet excitation energies at the ground-state geometry were calculated by time-dependent DFT (TD-DFT). Optimized excited-state geometry was calculated for the lowest singlet and two triplet states of A" symmetry by TD-DFT using Turbomole. For H, C, N, O, and Cl atoms, either polarized double-ζ basis sets[29] (G03) for geometry optimization and vibrational analysis, or cc-pvdz correlation consistent polarized valence double-ζ basis sets[30] (TD-DFT) were used, together with quasirelativistic effective core pseudopotentials and corresponding optimized set of basis functions for Re (all programs).[31] Double-ζ SVP basis was used for H, C, N, O, and Cl atoms in Turbomole. The difference density plots were drawn using the GaussView software.

III. Results

III.1. Electronic Structure, Low-Lying Excited States and Absorption Spectra. Hereafter, the following notation of electronic states is used: The prefix a, b, c. . . denotes the energy order of the excited states of given spin and symmetry. Thus, for example, a^1A' is the ground state, b^1A' is the first excited singlet state of the symmetry A', and $a^3A"$ is the lowest triplet state of the symmetry A", and so forth. The Kohn−Sham molecular orbitals reported in Tables S1−S6 of the Supporting Information were calculated without any symmetry constraints, but the aproximate symmetry within the C_s group is shown in parenthesis. Orbitals are numbered consecutively in the order of increasing energy, while the HOMO, LUMO notation is used in the text.

The spectroscopically most relevant KS molecular orbitals are the LUMO, HOMO, HOMO-1, and a lower-lying occupied π(bpy) orbital, which is HOMO-3 for L = Cl, py and HOMO-6 for L = I (Supporting Information Tables S1−S6). HOMO and HOMO-1 of the halide complexes are Re−L π-antibonding in character. The dπ(Re) contribution to these orbitals decreases from ∼50% to ∼30% on changing the chloride ligand for iodide. The pπ(halide) contribution concomitantly increases from ∼20% to ∼56%. For $[Re(py)(CO)_3(bpy)]^+$, HOMO and HOMO-1 are predominantly (60−66%) dπ(Re), mixed with π*(CO). The LUMO contains at least 90% π*(bpy). The lowest allowed electronic transition is identified as $a^1A' \rightarrow b^1A'$, which originates predominantly (93−99%) in the HOMO-1 → LUMO excitation (Supporting Information Tables S7 and S8). The $a^1A' \rightarrow b^1A'$ transition is manifested by a broad absorption band which occurs in CH_3CN at 340, 371, 375, and 384 nm for L = Etpy, Cl, Br, and I, respectively (Supporting Information Figures S1−S3). The b^1A' state has a $Re(CO)_3 \rightarrow$ bpy CT character for L = Etpy and $Re(L)(CO)_3 \rightarrow$ bpy CT for L = Cl, Br, and I. This is demonstrated in the left side of Figure 1 by maps of electron density differences upon excitation. The blue areas clearly show the depopulated regions around the Re and halide atoms. The halide → bpy contribution increases on going from L = Cl to Br and I due to increasing pπ(halide) participation in HOMO-1. This assignment of the lowest UV−vis absorption band agrees with previous calculations[32–35] and empirical considerations based on the molar absorptivity, solvatochromism or resonance Raman enhancement.[17,18,36–39] The lowest-lying $a^1A' \rightarrow a^1A"$ MLCT transition, which originates in HOMO → LUMO excitation, is very weak because of lack of overlap between the depopulated d(π) and π* orbitals involved (Supporting Information Tables S7 and S8). It may, at most, weakly contribute to the red tail of the absorption band.

Three triplet excited states were calculated to occur in a narrow (0.3−0.5 eV wide) energy range (Supporting Information Tables S9 and S10). Triplet TD-DFT calculations were validated by comparing calculated and experimental excited-state IR spectra[33,34,37,40] of the lowest excited-state for L = Cl and Etpy. The best agreement was obtained using the B3LYP functional. The CH_3CN solvent modeled by COSMO was included in calculations of the halide complexes. For $[Re(py)(CO)_3(bpy)]^+$, a good match of the IR spectra was obtained only for calculations in vacuum (the amount of the calculated IL admixture increases when the CH_3CN solvent is included by continuum

(20) Frisch, M. J., Trucks, G. W.; Schlegel, H. B.; Scuseria, G. E.; Robb, M. A.; Cheeseman, J. R. ; J. A. Montgomery, J.; Vreven, T.; Kudin, K. N. ; Burant, J. C.; Millam, J. M.; Iyengar, S. S.; Tomasi, J.; Barone, V.; Mennucci, B.; Cossi, M.; Scalmani, G.; Rega, N.; Petersson, G. A.; Nakatsuji, H.; Hada, M.; Ehara, M.; Toyota, K.; Fukuda, R.; Hasegawa, J.; Ishida, M.; Nakajima, T.; Honda, Y. ; Kitao, O.; Nakai, H.; Klene, M.; Li, X.; Knox, J. E.; Hratchian, H. P.; Cross, J. B.; Bakken, V.; Adamo, C.; Jaramillo, J.; Gomperts, R.; Stratmann, R. E.; Yazyev, O.; Austin, A. J.; Cammi, R.; Pomelli, C.; Ochterski, J. W.; Ayala, P. Y.; Morokuma, K.; Voth, G. A.; Salvador, P.; Dannenberg, J. J.; Zakrzewski, V. G.; Dapprich, S.; Daniels, A. D.; Strain, M. C.; Farkas, O.; Malick, D. K.; Rabuck, A. D.; Raghavachari, K.; Foresman, J. B.; Ortiz, J. V.; Cui, Q.; Baboul, A. G.; Clifford, S.; Cioslowski, J.; Stefanov, B. B.; Liu, G.; Liashenko, A.; Piskorz, P.; Komaromi, I.; Martin, R. L.; Fox, D. J.; Keith, T.; Al-Laham, M. A.; Peng, C. Y.; Nanayakkara, A.; Challacombe, M.; Gill, P. M. W.; Johnson, B.; Chen, W.; Wong, M. W.; Gonzalez, C.; Pople, J. A. , *Gaussian 03*, revision C.02; Gaussian, Inc.: Wallingford, CT, 2004.
(21) Ahlrichs, R.; Bär, M.; Häser, M.; Horn, H.; Kölmel, C. *Chem. Phys. Lett.* **1989**, *162*, 165.
(22) Ahlrichs, R.; Bär, M.; Baron, H. P.; Bauernschmitt, R.; Böcker, S.; Deglmann, P.; Ehrig, M.; Eichkorn, K.; Elliott, S.; Furche, F.; Haase, F.; Häser, M.; Horn, H.; Hättig, C.; Huber, C.; Huniar, U.; Kattannek, M.; Köhn, A.; Kölmel, C.; Kollwitz, M.; May, K.; Ochsenfeld, C.; Öhm, H.; Patzelt, H.; Rubner, O.; Schäfer, A.; Schneider, U.; Sierka, M.; Treutler, O.; Unterreiner, B.; von Arnim, M.; Weigend, F.; Weis, P.; Weiss, H. *TURBOMOLE V5−7*; Quantum Chemistry Group, University of Karlsruhe, Karlsruhe, Germany, 2004.
(23) Becke, A. D. *J. Chem. Phys.* **1993**, *98*, 5648.
(24) Perdew, J. P.; Burke, K.; Ernzerhof, M. *Phys. Rev. Lett.* **1996**, *77*, 3865.
(25) Adamo, C.; Barone, V. *J. Chem. Phys.* **1999**, *110*, 6158.
(26) Cossi, M.; Rega, N.; Scalmani, G.; Barone, V. *J. Comput. Chem.* **2003**, *24*, 669.
(27) Klamt, A.; Schüürmann, G. *J. Chem. Soc., Perkin Trans. 2* **1993**, 799.
(28) Klamt, A.; Jones, V. *J. Chem. Phys.* **1996**, *105*, 9972.
(29) Hariharan, P. C.; Pople, J. A. *Theo. Chim. Acta* **1973**, *28*, 213.
(30) Woon, D. E.; Dunning, T. H., Jr. *J. Chem. Phys.* **1993**, *98*, 1358.
(31) Andrae, D.; Häussermann, U.; Dolg, M.; Stoll, H.; Preuss, H. *Theor. Chim. Acta* **1990**, *77*, 123.
(32) Vlček, A., Jr.; Záliš, S. *J. Phys. Chem. A* **2005**, *109*, 2991.
(33) Vlček, A., Jr.; Záliš, S. *Coord. Chem. Rev.* **2007**, *251*, 258.
(34) Dattelbaum, D. M.; Martin, R. L.; Schoonover, J. R.; Meyer, T. J. *J. Phys. Chem. A* **2004**, *108*, 3518.
(35) Martin, R. L. *J. Chem. Phys.* **2003**, *118*, 4775.
(36) Kalyanasundaram, K. *J. Chem. Soc., Faraday Trans. 2* **1986**, *82*, 2401.
(37) Liard, D. J.; Busby, M.; Matousek, P.; Towrie, M.; Vlček, A., Jr. *J. Phys. Chem. A* **2004**, *108*, 2363.
(38) Smothers, W. K.; Wrighton, M. S. *J. Am. Chem. Soc.* **1983**, *105*, 1067.
(39) Stufkens, D. J.; Vlček, A., Jr. *Coord. Chem. Rev.* **1998**, *177*, 127.
(40) Blanco-Rodríguez, A. M.; Gabrielsson, A.; Motevalli, M.; Matousek, P.; Towrie, M.; Šebera, J.; Záliš, S.; Vlček, A., Jr. *J. Phys. Chem. A* **2005**, *109*, 5016.

Table 1. Selected TD-DFT (B3LYP) Calculated Structural Parameters of the a^1A' (ground), b^1A', b^3A'', and a^3A'' states of $[Re(Cl)(CO)_3(bpy)]^+$ and $[Re(py)(CO)_3(bpy)]^{+a}$

	$[Re(Cl)(CO)_3(bpy)]$ in CH_3CN (COSMO)							$[Re(py)(CO)_3(bpy)]^+$ in vacuum						
bond lengths, Å	a^1A'	b^1A'	%(S−G)	a^3A''	%(T_a−S)	b^3A''	%(T_b−S)	a^1A'	b^1A'	%(G−S)	a^3A''	%(T_a−S)	b^3A''	%(T_b−S)
Re−N	2.232	2.211	−0.9	2.173	−1.7	2.227	0.7	2.233	2.198	−1.6	2.163	−1.6	2.226	1.3
Re−L	2.533	2.455	−3.1	2.456	0.0	2.505	2.0	2.294	2.272	−1.0	2.275	0.1	2.286	0.6
Re−C_{ax}	1.938	1.972	1.8	1.986	0.7	1.948	−1.2	1.959	1.977	0.9	2.001	1.2	1.976	−0.1
Re−C_{eq}	1.944	1.978	1.7	1.985	0.4	1.956	−1.1	1.955	2.012	2.9	1.997	−0.7	1.969	−2.1
N−C6	1.343	1.345	0.1	1.353	0.6	1.327	−1.3	1.346	1.350	0.3	1.356	0.4	1.329	−1.6
N−C2	1.356	1.390	2.5	1.398	0.6	1.402	0.9	1.360	1.390	2.2	1.404	1.0	1.398	0.6
C2−C2′	1.482	1.438	−3.0	1.427	−0.8	1.41	−1.9	1.483	1.435	−3.2	1.425	−0.7	1.413	−1.5
C−O_{ax}	1.160	1.151	−0.8	1.148	−0.3	1.157	0.5	1.149	1.142	−0.6	1.140	−0.2	1.146	0.4
C−O_{eq}	1.157	1.152	−0.4	1.151	−0.1	1.157	0.4	1.152	1.143	−0.8	1.145	0.2	1.149	0.5
						angles, (deg)								
N1−Re−N2	73.9	76.0	2.8	76.6	0.9	74.4	−2.1	73.9	76.3	3.2	77.2	1.2	74.3	−2.6
C_{eq}−Re−C_{eq}	89.8	95.6	6.5	86.2	−9.8	89.1	−6.8	90.1	92.8	3.0	85.2	−8.2	88.1	−5.1
L−Re−C_{ax}	175.3	179.6	2.5	174.8	−2.7	174.2	−3.1	177.8	176.4	−0.8	174.7	−1.0	176.4	0.0
N−Re−L	83.4	88.5	6.1	87.9	−0.8	83.2	−6.0	86.1	85.3	−0.9	85.2	−0.1	85	−0.4
N−Re−C_{ax}	92.9	91.7	−1.3	88.1	−3.9	92.2	0.5	92.1	92.1	0.0	90.7	−1.5	92.1	0.0

[a] %(S−GS), %(T_b−S), and %(T_a−S) are the percent change in the given parameter between b^1A' and a^1A', b^3A'' and b^1A', and a^3A'', and b^1A' states, respectively. Results obtained with the PBE0 functional are shown in Table S11 of the Supporting Information.

models). Because of the close proximity of the triplet states in the Etpy complex, the IL contribution to the lowest triplet state is unrealistically exaggerated in B3LYP/CPCM calculations, predicting wrong IR excited-state spectra.) The lowest triplet state in all three complexes was identified as a^3A''. Originating predominantly in HOMO → LUMO excitation, the a^3A'' state can be qualitatively viewed as mostly $Re(CO)_3$ → bpy and $Re(L)(CO)_3$ → bpy CT for L = Etpy and L = halide, respectively. The L → bpy contribution increases in the order Cl < Br < I. The a^3A'' state contains a smaller but significant, admixture of π(bpy) → π^*(LUMO) intraligand excitation (IL). Both the CT and IL contributions are clearly seen in calculated changes of electron density upon excitation (Figure 1, right). The second triplet state a^3A' is almost pure HOMO-1 → LUMO CT excitation. The third triplet, b^3A'', is approximately isoenergetic with the optically populated singlet state b^1A'. It is predominantly a $\pi \rightarrow \pi^*$(bpy) IL state, with a smaller contribution from the HOMO → LUMO CT excitation (Figure 1, right).

Table 1 summarizes the B3LYP-optimized geometries of the a^1A' ground state, and the b^1A', b^3A'', and a^3A'' excited states of $[Re(Cl)(CO)_3(bpy)]$ and $[Re(py)(CO)_3(bpy)]^+$, which are useful to understand the ISC, as will be seen later (For geometries obtained with PBE0, see Supporting Information Table S11). The calculations predict that excitation to b^1A' mostly affects the bonds within the bpy ligand. The largest changes concern the C2−C2′ and N−C2 bonds, which shorten and lengthen, respectively. Moreover, the Re−N(bpy), Re−L, and C≡O bonds contract upon excitation while Re−C bonds elongate, and the skeletal angles C_{eq}−Re−C_{eq}, N−Re−N, Cl−Re−C_{ax}, and Cl−Re−N open. The calculations agree with resonance Raman spectra of $[Re(Cl)(CO)_3(bpy)]$, $[Re(Etpy)(CO)_3(bpy)]^+$ and similar complexes, which show enhancement of Raman peaks due to ν(CC) and ν(NC), ν(CO), ν(ReN), ν(Re-halide), and $\delta Re(CO)_3$ vibrations.[18,37,38] Concerning the singlet−triplet differences, Table 1 shows that for both b^3A'' and a^3A'', the largest geometry changes involve skeletal bond angles around the Re atom and some of the Re-ligand bond lengths. The largest change occurs in the C_{eq}−Re−C_{eq} angle. Depending on the particular triplet, the skeletal bond angles N−Re−N, N−Re−Cl, L−Re−C_{ax}, N−Re−C_{ax}, and, to a lesser extent, the Re−C, Re−Cl, and Re−N(bpy) bond distances also have different values in the singlet and triplet excited states. The intra-bpy bonds differ very little for a^3A'', whereas, for b^3A'', calculations predict significant differences in the C2−C2′ and N−C6 bonds. Interestingly, the calculated small contraction of the Re−N(bpy) bond (0.06−0.07 Å) on going from the ground to the a^3A'' state agrees well with the value of ∼0.04 Å, measured for the ^{3}MLCT state of $[Ru^{II}(bpy)_3]^{2+}$ by picosecond X-ray absorption spectroscopy.[41]

III.2. Time-Resolved Fluorescence Spectroscopy. Figure 2 shows a typical 2D time-wavelength luminescence data measured up to 3 ps time delay after 400 nm excitation for the investigated complexes in CH_3CN solution. All plots show a broad and short-lived luminescence centered around 500−550 nm, followed by a longer-lived red-shifted component. Cuts at fixed times provide time-dependent luminescence spectra, which are shown in Figure 3 for the case of $[Re(I)(CO)_3(bpy)]$, whereas cuts at fixed luminescence wavelengths provide the kinetic traces, shown in Figure 4. The same results for all other complexes are shown in Supporting Information Figures S4 and S5. The general trends can be summarized as follows:

The broad luminescence band centered around 500−550 nm is immediately present at zero time delay. The band covers most of the visible spectral region, extending beyond 650 nm. We attribute it to fluorescence, based on the fact that it lies to the red of the singlet absorption band and appears promptly.

The fluorescence band decays rapidly, and is replaced by a band at longer wavelengths at 600−610 and 580 nm for L = Cl, I, Br, and Etpy, respectively. This new band remains at the same energy up to the longest recorded time delays, i.e., 150 ps (not shown). It is identified as phosphorescence, since it lies at the same position as the steady-state phosphorescence band.[17,18,42]

The kinetic traces confirm the presence of a short-lived decay component in the blue side of the spectrum, and a longer-lived one on the red side. These are nonexponential dependences, and the analysis below identifies the decay times involved.

From the above, it is clear that there are at least two luminescence bands in the spectra, but more contributions cannot be excluded. Therefore, in order to spectrally isolate the luminescence components, we have applied two approaches:

(41) Gawelda, W.; Johnson, M.; de Groot, F. M. F.; Abela, R.; Bressler, C.; Chergui, M. *J. Am. Chem. Soc.* **2006**, *128*, 5001.
(42) Blanco-Rodríguez, A. M.; Ronayne, K. L.; Záliš, S.; Sýkora, J.; Hof, M.; Vlček, A., Jr. *Phys. Chem. B*, **2008**, *112*, 3506.

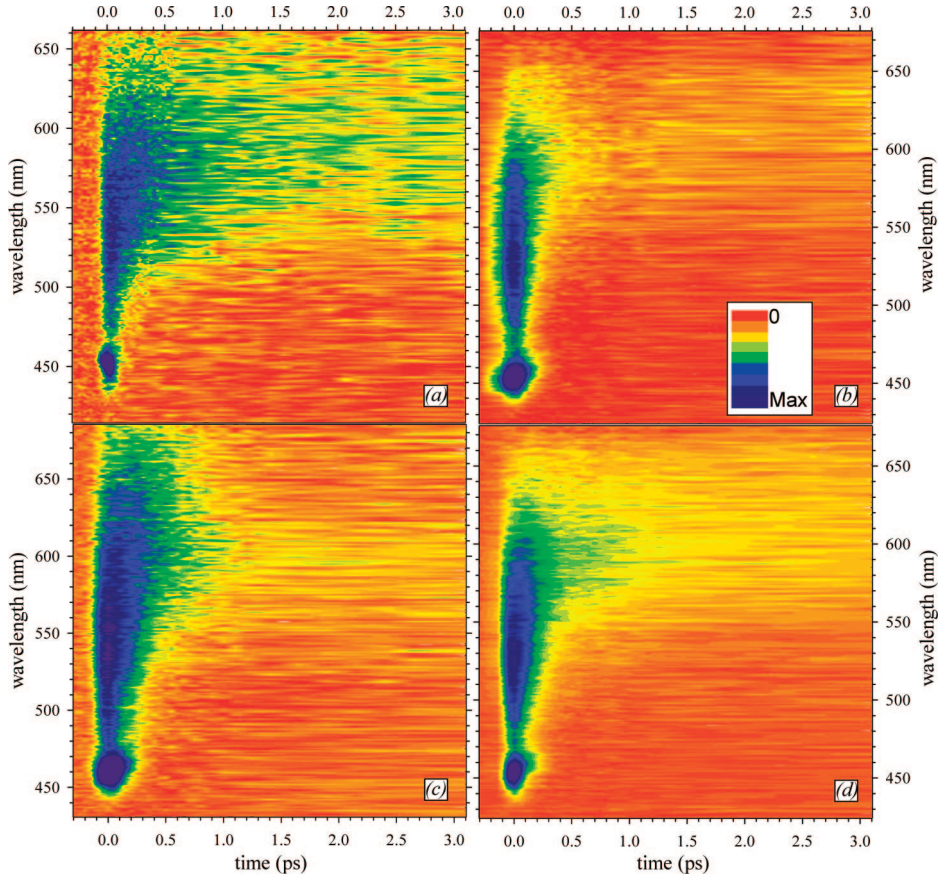

Figure 2. 2D plots of time-resolved luminescence spectra of $[Re(L)(CO)_3(bpy)]^n$ in CH_3CN, measured after 400 nm excitation. (a): L = Etpy; (b): L = Cl; (c): L = Br, (d): L = I. Intensities are color-coded. The peak at 457 nm is a CH_3CN Raman line.

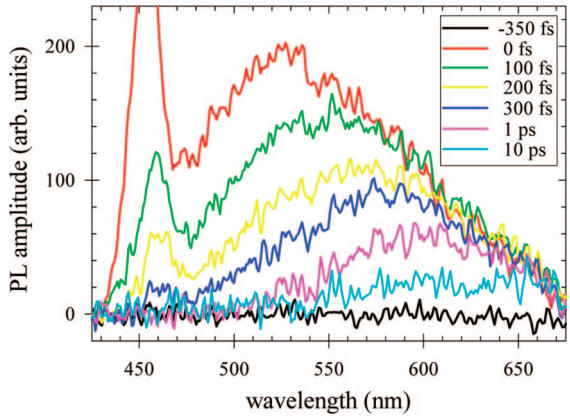

Figure 3. Luminescence spectra of $[Re(I)(CO)_3(bpy)]$ in CH_3CN measured at selected time delays upon 400 nm excitation. The signal at ~457 nm is the CH_3CN Raman line.

(a) A global (simultaneous) (GF) fit of kinetic traces averaged over 10 nm steps of the luminescence spectra using eq 1:

$$I = \{A_1 e^{(-t/\tau_1)} + A_2 e^{(-t/\tau_2)} + A_3[e^{(-t/\tau_{ph})} - e^{(-t/\tau_3)}]\} \otimes e\left[-\left(\frac{t-t_0}{0.6*\Delta_{IRF}}\right)^2\right] \quad (1)$$

in which we assume three characteristic times (τ_1, τ_2, and τ_{ph}) and a rising component for the phosphorescence (τ_3). The last Gaussian term describes the convolution with the instrument response function (IRF), where Δ_{IRF} and t_0 are its fwhm and the time zero, respectively. In the GF procedure, the time constants have been considered as common kinetic parameters at all wavelengths, whereas the amplitudes A_1 to A_3 have been determined for each wavelength. Given that the phosphorescence lifetime is very long (40−200 ns)[18,42] compared to the actual time scales measured here, we can consider the third term in eq 1 to be ~1. The fitted time profiles of the luminescence intensity are shown in Figure 4 for a few selected luminescence

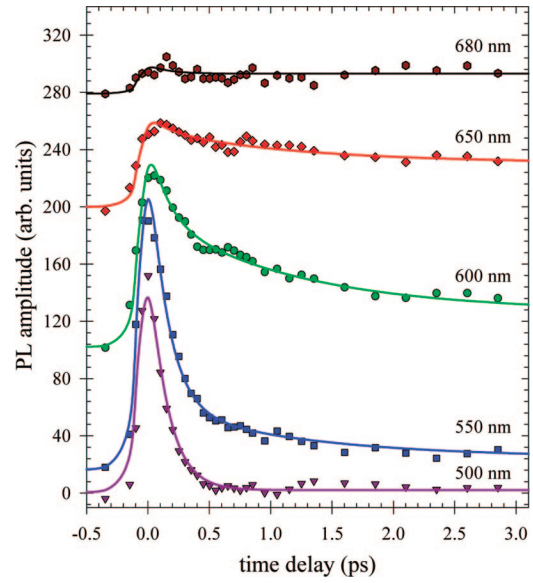

Figure 4. Time profiles of luminescence of $[Re(I)(CO)_3(bpy)]^+$ in CH_3CN, measured at different wavelengths following 400 nm, ~80 fs excitation.

Table 2. Fluorescence Decay Lifetimes (in fs) of $[Re(L)(CO)_3(bpy)]^n$ and Estimated[a] Spin-Orbit Coupling Energies (in cm^{-1})

L	τ_1	τ_2	SO $b^1A'-b^3A''$	SO $b^1A'-a^3A''$
Etpy	130 ± 20	870 ± 80	58	550
Cl	85 ± 8	340 ± 50	92	503
Br	128 ± 12	470 ± 50		
I	152 ± 8	1180 ± 150	267	1303

[a] Using B3LYP-calculated KS molecular orbitals and electronic transitions (Tables S1,3, and 5 of the Supporting Information); b^1A' of all complexes and triplets for L = Cl and I were calculated in CH_3CN, triplets for L = py in vacuum.

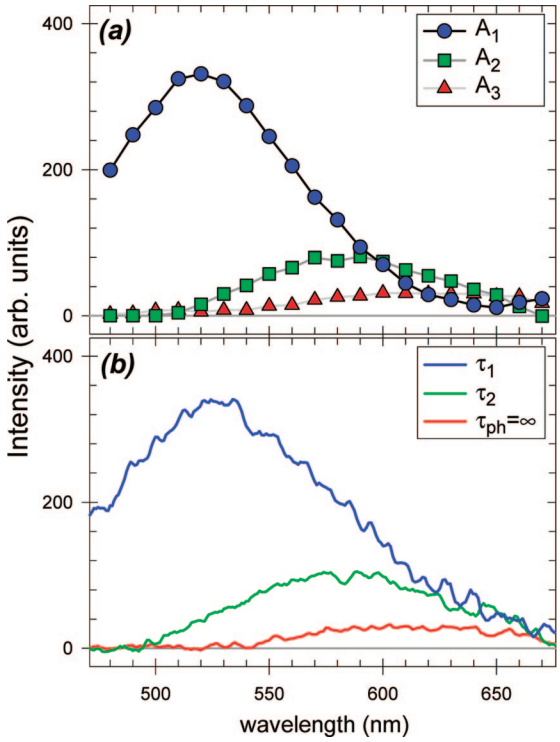

Figure 5. (a) Pre-exponential factors A_1, A_2 and A_3 obtained by a global fit of eq. 1 to time traces of luminescence intensity measured from $[Re(I)(CO)_3(bpy)]$ in CH_3CN. Luminescence signals were averaged over 10 nm intervals. (b) Decay associated spectra for the same sample obtained from an SVD-Global analysis (see SI for details). The reported spectra, labelled τ_1, τ_2, and τ_{ph}, have been assigned to the respective decay components of eq. 1. $\tau_{ph} = \infty$ the third component belongs to the long-lived phosphorescence.

wavelengths of $[Re(I)(CO)_3(bpy)]$, showing that additional components are not necessary to improve the quality of the fit. The derived time constants of all complexes are reported in Table 2. In this table, the rising τ_3 component is not shown as it turned out to be equal to the τ_1 decay constant. This observation points to the fluorescence feeding the phosphorescence in a direct fashion. By plotting the preexponential factors obtained for each time constant, as a function of luminescence wavelength, we can identify the spectral components associated to the various decay times. The result is shown in Figure 5a for $[Re(I)(CO)_3(bpy)]$. It is clear from this picture that there are three luminescence bands contributing to the time-dependent spectra. The red-most one is obviously the phosphorescence, while the blue-most is the fluorescence band, which is predominant and, due to its width, extends over all wavelengths. An intermediate spectral feature associated with the τ_2 decay constant shows up around 590 nm. Similar spectral decompositions, always delivering three components, were obtained for all other complexes (see Supporting Information Figure S6).

(b) The results derived from the kinetic fits are confirmed by a finer analysis based on singular value decomposition (SVD) and global analysis (GA). Details of the procedure are given in the Supporting Information. Briefly, this analysis allows us to extract from the 2-D time-wavelength matrix (Figure 2) the minimal number of spectral components, related to the kinetics components, necessary to describe the entire spectral and temporal evolution of the system. A GA of these kinetics has provided time constants identical (within errors bars) to those from the direct fit (Table 2). In this analysis, we take a kinetic model, assuming that the second luminescent state and the phosphorescent state are both populated from the initially excited singlet state and that the second state undergoes conversion to the phosphorescent state. An example of the quality of the fit of kinetic traces is shown in Supporting Information Figure S7d at three characteristic luminescence wavelengths. The spectra associated with the three decay constants in $[Re(I)(CO)_3(bpy)]$, obtained by SVD-GA, are shown in Figure 5b, and they fully agree with the above analysis. The decay associated spectra (DAS) of the other complexes are shown in Supporting Information Figure S8. The results of the SVD-GA fully confirm the pattern of three emitting states in all Re complexes.

III.3. Estimate of Spin−Orbit Coupling Strength. The optically prepared singlet excited state b^1A' and the triplet states b^3A'' and a^3A'' have different symmetries, the depopulated HOMO-1 and HOMO orbitals being oriented perpendicularly. This means that the first-order SO coupling and, hence, the $b^1A' \rightarrow b^3A''$ and $b^1A' \rightarrow a^3A''$ ISCs are symmetry-allowed, the direct product $A' \otimes A''$ transforming as rotation. This is shown in Figure 1, where the singlet and triplet states are represented by difference electron density maps, calculated by TD-DFT. However, the second triplet, a^3A', is not considered because the $b^1A' \rightarrow a^3A'$ ISC and the $b^3A'' \rightarrow a^3A'$ internal conversion are symmetry and overlap forbidden, respectively.

The magnitude of the spin−orbit coupling term $\langle b^1A'|\hat{H}_{SO}|a^3A''\rangle$ was roughly estimated from the DFT data, assuming that only the Re and halogen atoms contribute. This simple approach[43] allows us to express the SO integrals as $ab(-i/2)\xi_{Re}(c'_d c''_d)$ and $ab(-i/2)(\xi_{Re}c'_d c''_d + \xi_X c'_p c''_p)$ for $[Re(py)(CO)_3(bpy)]^+$ and $[Re(X)(CO)_3(bpy)]$ (X = Cl, I), respectively, where c'_d and c'_p are the d and p orbital coefficients in the HOMO-1, while c''_d and c''_p are the corresponding coefficients in the HOMO, ξ is the atomic spin−orbit parameter (2200, 586, and 5060 cm^{-1} for Re, Cl, and I, respectively[44]), and a and b are the weights of the HOMO-1 → LUMO and HOMO → LUMO excitations in the transitions to the b^1A' and a^3A'' states, respectively. The term $\langle b^1A|\hat{H}_{SO}|b^3A''\rangle$ can be estimated in the same way, using b equals to the weight of the HOMO → LUMO excitation in the $a^1A' \rightarrow b^3A''$ transition. The estimated SO coupling constants are listed in Table 2.

IV. Discussion

The above results can be summarized in the following points, which will be discussed in more detail:

−We identify three spectral components in the luminescence spectrum of Re-based complexes recorded at very short times (fs−ps). In addition to the short-lived blue-most fluorescence

(43) Ballhausen, C. J. *Introduction to Ligand Field Theory*; McGraw-Hill, Inc.: New York, 1962.
(44) Khudyakov, I. V.; Serebrennikov, Y. A.; Turro, N. J. *Chem. Rev.* **1993**, *93*, 537.

Scheme 1. Excited-State Dynamics of $[Re(L)(CO)_3(bpy)]^n$ Complexes [a]

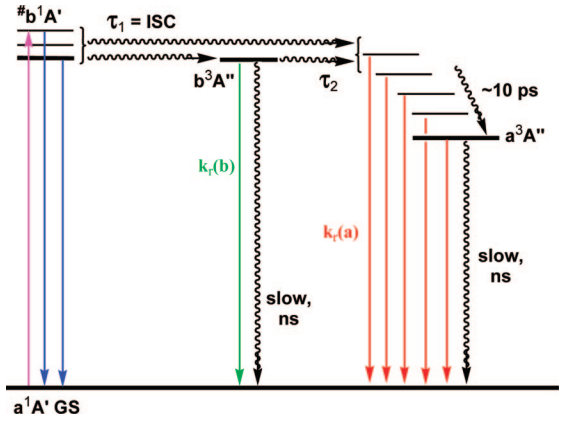

[a] Color code: light absorption to b^1A' in violet, fluorescence in blue, b^3A'' phosphorescence in green, and a^3A'' phosphorescence in red (# denotes vibrational excitation).

band and the red-most long-lived phosphorescence band, an intermediate band shows up with typical lifetimes of 0.3 to 1.2 ps.

−ISC in Re carbonyl−bipyridine complexes is ultrafast, though the rates are slower than those in the previously studied Ru− and Fe−tris-bipyridines,[6,7] in which the metal atom has a smaller SO constant.

−The ISC rates in the halogenated complexes do not scale with the strength of the SO coupling and the SO constant of the ligand L.

−The optically populated excited-state is b^1A' with a mixed $Re(CO)_3 \rightarrow$ bpy and halide $\rightarrow$ bpy CT character. The halide participation increases in the sequence Cl < Br < I. The two spectroscopically relevant triplet states are a^3A'' and b^3A'', which have predominant CT and IL(bpy) characters, respectively.

Before discussing the details of the relaxation processes, it is important to identify the intermediate band. We attribute it to luminescence from the triplet b^3A'' state, on the basis of the following arguments:

(1) It cannot be a fluorescence in spite of its short lifetime because the transition to the lowest lying singlet state a^1A'' is, as already mentioned, overlap-forbidden and, hence, very weakly excited from the ground state.

(2) The most likely candidates would either be a hot luminescence from the lowest phosphorescent triplet state a^3A'' or a higher lying triplet state. The hot luminescence is unlikely on the basis of the changing area under the bands. In addition, the red wing of the luminescence (phosphorescence) remains unchanged over time (Figure 3), whereas a narrowing would be expected in the case of hot phosphorescence.

(3) As discussed above (see also Supporting Information Tables S7−S10), two quasi-degenerate triplet states (a^3A' and b^3A'') occur close to the singlet state, while the third is the lowest lying one (a^3A''). As already mentioned, the optically prepared singlet state can only be coupled to the b^3A'' and a^3A'' states by spin−orbit interaction, while the second triplet a^3A' is not involved. Thus, the only higher lying triplet state that can be populated by ISC from the singlet state is the b^3A'' state. We therefore attribute the intermediate luminescence band to this state.

On the basis of the above assignment of the three emitting states, and on the kinetic model used in the SVD-GF, we propose the excited-state relaxation model shown in Scheme 1, which rationalizes the temporal evolution of the luminescence spectra in terms of population and relaxation of the singlet b^1A' and two triplet (b^3A'' and a^3A'') excited states:

(a) Optical excitation prepares the b^1A' excited state, which undergoes fluorescence, and is short-lived due to efficient ISC (rate $= 1/\tau_1$) to the triplet b^3A'' and a^3A'' excited states. The fluorescence promptly appears upon excitation, with a Stokes shift of $\sim$6000 cm^{-1} with respect to the excitation energy.

(b) The risetime of the lowest a^3A'' phosphorescence reflects the decay time of the fluorescence, even at its red-most wing. The phosphorescence then does not evolve with time. This suggests that the a^3A'' state is initially populated over a broad range of vibrational levels, most likely low-frequency skeletal modes, which have little effect on the band profile (see below). The ensuing relaxation, which involves energy dissipation to the first solvation layer and then into the bulk solvent, is known to occur in CH_3CN with two lifetimes of about 1 and 10 ps, respectively.[37,42] Low-frequency vibrations are only weakly, if at all, coupled to the phosphorescence, as was observed in the case of $[Ru^{II}(bpy)_3]^{2+}$.[6] Their cooling thus has only small effects on the shape or position of the luminescence band, in agreement with the lack of spectral evolution of the red-most wing.

(c) The population of the upper state b^3A'' also occurs at a rate of $(\tau_1)^{-1}$. As a high-lying, predominantly ^{3}IL state, b^3A'' is expected to have a long intrinsic lifetime, probably in the hundreds of ns. The observed τ_2 decay is thus attributed entirely to the conversion into high vibrational levels of the lower state a^3A''. This implies that they should show a solvent dependence.[42] A solvent dependence study is underway, and our preliminary measurements in DMF do show the expected trend, whereby the τ_2 value increases from 340 ± 50 fs (L = Cl) and 470 ± 50 fs (L = Br) in CH_3CN to 1420 ± 90 and 1600 ± 200 fs, respectively, as the diffusional solvent relaxation time increases from 630 to 1700 fs.[45] In this picture, the phosphorescence from the a^3A'' state should contain an additional rise on a time scale of τ_2, but the expected small change of an already weak signal seems to be canceled by the overlapping decay of the fluorescence (τ_1) and the intermediate phosphorescence (τ_2). In addition, it may be convoluted with additional and longer vibrational relaxation processes taking place in the a^3A'' state.

Having established the nature of the intermediate state and the photophysical mechanism (Scheme 1), we now turn our attention to the ISC proper. ISC in $[Re(L)(CO)_3(bpy)]^n$ occurs on a time scale (τ_1) of 80 to 160 fs (Table 2). Figure 1 shows that the change in the spin momentum upon ISC is accompanied by a change in the angular momentum, which is accomplished by rotating the depopulated orbital. The total momentum is thus conserved, making ISC allowed by first-order spin−orbit coupling. In a way, this is an inorganic manifestation of the El-Sayed rules, well-known in organic photophysics.[46]

For the halogenated complexes, the ISC rate runs in a markedly opposite trend to the SO coupling constant of the ligand L. Furthermore, even the fastest ISC recorded here for $[Re(Cl)(CO)_3(bpy)]$ is much slower than the $\sim$20 fs ISC determined[6,7] for the $[M^{II}(bpy)_3]^{2+}$ (M = Ru, Fe) complexes with weaker SO constants of the metal atom. We propose that the SO interaction in all of these complexes is strong enough to provide sufficient electronic coupling and its variations with the metal no longer affect the ISC rate. Instead, ISC is governed

(45) Horng, M. L.; Gardecki, J. A.; Papazyan, A.; Maroncelli, M. *J. Phys. Chem.* **1995**, *99*, 17311.
(46) Turro, N. J. *Modern Molecular Photochemistry*; Benjamin/Cummings Publishing Co.: Menlo Park, 1978.

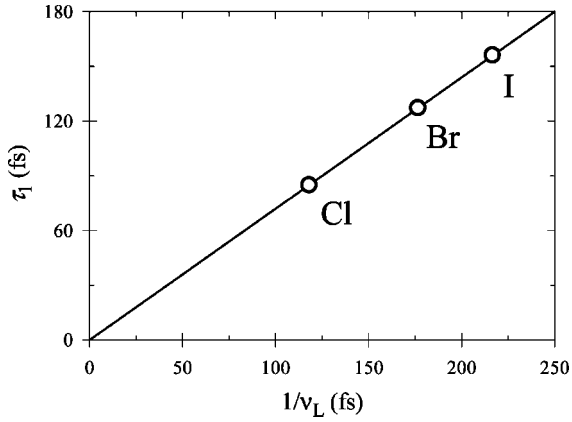

Figure 6. Correlation of the ISC times measured in this work for the $[Re(L)(CO)_3(bpy)]$ (L = Cl, Br, I,) complexes with the vibrational period of the Re−L stretch mode in similar $[Re(L)(CO)_3(iPr{-}N{=}CH{-}CH{=}N{-}iPr)]$ complexes, as derived from their resonance Raman spectra.[18]

by factors, such as the shapes of the singlet and triplet potential energy surfaces in their crossing region and, eventually also, the availability of optically driven vibrational modes to explore it.[7] Thus, it is the position in energy and shape of the ground, singlet and triplet surfaces, which are the real tuning parameters that determine ISC rates in the complexes studied in this and previous work.[6,7] These potential energy surfaces depend on the nature and composition of ligands bound to the metal atom, which would explain the dramatic variations found between the Re complexes here and the $[M^{II}(bpy)_3]^{2+}$ (M = Ru, Fe) complexes.[6,7]

In the case of the present Re complexes, the ISC times are in the range of vibrational periods of the low frequency modes. In fact, there is a strong correlation between them, as can be seen in Figure 6. For the case of the Re−Etpy mode, the available resonance Raman spectra do not show a clear band in the frequency region of interest,[37] and it is not even clear which mode should at all be involved. The correlation of Figure 6 may be fortuitous, but it is remarkable how well it relates the counterintuitive trends of the ISC times with a known physical parameter of the system, the Re−L vibration frequency, suggesting that the latter may mediate the ISC in Re−halide complexes. If this is so, then the ISC occurs in a strongly nonadiabatic regime, as the change of spin takes place in less than a complete Re−L oscillation. Under such a situation, the region of strong singlet−triplet interaction will be in the first place explored by vibrations that are optically driven. In the Re−halogen complexes, the light-induced charge transfer withdraws electron density mainly from the $Re(L)(CO)_3$ moiety. This will undoubtedly affect the field of forces within this moiety, activating the low-frequency skeletal modes, which will modulate the ISC accordingly. It may also explain why other modes, present in the resonance Raman spectrum, do not affect the ISC process.

We still need to explain why the b^3A'' state is populated as efficiently from the singlet state as the a^3A'' state, even though the SO coupling to both is so different (Table 2). Given that it is a predominantly ligand-centered state, one cannot exclude that in this case, other, higher frequency modes mediate the ISC, compensating for the weaker SO coupling with the singlet state. Last, the singlet excitation energy is almost isoenergetic with the GS → b^3A'' vertical excitation energy.

V. Conclusions

Femtosecond fluorescence up-conversion with polychromatic detection allowed us to identify the relaxation pathways in $[Re(L)(CO)_3(bpy)]^n$ (L = Etpy, Cl, Br, I) complexes dissolved in acetonitrile. The initially excited singlet state undergoes ISC to two triplet states simultaneously with a common time constant in the range 85−160 fs, which shows a dependence on L. The singlet and triplet states involved differ in the orientation of the depopulated orbital, making ISC allowed by first-order SO coupling.

We find that the ISC occurs in a strongly nonadiabatic regime. We believe that the spin−orbit coupling is saturated, but the remarkable correlation of the ISC times with the period of the Re−L modes suggests that ISC is modulated by low-frequency skeletal vibrations of the $Re(L)(CO)_3$ unit. However, the SO coupling strength does become an ISC rate limiting factor in those complexes where it is weaker than some critical value because of symmetry constraints. This is the case of Pt(II) and Cu(I) phosphine complexes,[10,11] where slow (picosecond) ISC rates correlate with rather small SO coupling energies, 25−50 cm^{-1}. More studies are needed to fully characterize the nature of ultrafast ISC in metal complexes.

The singlet-state lifetimes in Re^I carbonyl−bipyridine complexes are long enough to be utilized for ultrafast electron or energy transfer in supramolecular assemblies, at surfaces or molecule/nanoparticle interfaces. Indeed, a "hot electron injection" into TiO_2 has been reported.[47,48]

Acknowledgment. Financial support is gratefully acknowledged from the Swiss National Science Foundation (Contract Nos. 200021-107956 and 200021-105239), the EPSRC and STFC (CMSD43), COST Action D35, the ESF-DYNA programme, and the Ministry of Education of the Czech Republic (grants 1P05OC68 and OC139). Access to the META Centrum computing facilities was provided under the research intent MSM6383917201.

Supporting Information Available: For all complexes investigated in this article: (a) Steady-state UV−vis absorption spectra and their comparison with the calculated oscillator strengths; (b) fluorescence up-conversion spectra and kinetic traces; (c) tables of the calculated one-electron energies and compositions of spectroscopically relevant Kohn−Sham molecular orbitals; (d) tables of the calculated singlet electronic transitions with oscillator strength larger than 0.001; (e) Tables of the calculated low-lying triplet electronic transitions; (f) a table of the calculated structural parameters of the a^1A' (ground), b^1A' and a^3A'' states of $[Re(Cl)(CO)_3(bpy)]$ and $[Re(py)(CO)_3(bpy)]^{+}$; (g) method to extract the spectral component by a global fit of kinetic traces at different emission wavelengths; (h) description of the singular value decomposition (SVD) and of the global analysis (GA); and (i) complete refs 20 and 22. This material is available free of charge via the Internet at http://pubs.acs.org.

JA710763W

(47) Wang, Y.; Asbury, J. B.; Lian, T. *J. Phys. Chem. A* **2000**, *104*, 4291.
(48) Asbury, J. B.; Hao, E.; Wang, Y.; Ghosh, H. N.; Lian, T. *J. Phys. Chem. B* **2001**, *105*, 4545.